

D.V. Bugg,  
Queen Mary, University of London, London E1 4NS, UK

### Abstract

A partial wave analysis of PS185 data for  $\bar{p}p \rightarrow \bar{\Lambda}\Lambda$  is presented. A  $^3S_1$  cusp is identified in the inverse process  $\bar{\Lambda}\Lambda \rightarrow \bar{p}p$  at threshold, using detailed balance to deduce cross sections from  $\bar{p}p \rightarrow \bar{\Lambda}\Lambda$ . Partial wave amplitudes for  $\bar{p}p$   $^3P_0$ ,  $^3F_3$ ,  $^3D_3$  and  $^3G_3$  exhibit a behaviour very similar to resonances observed in Crystal Barrel data. With this identification, the  $\bar{p}p \rightarrow \bar{\Lambda}\Lambda$  data then provide evidence for a new  $I = 0$ ,  $J^{PC} = 1^{--}$  resonance with mass  $M = 2290 \pm 20$  MeV,  $\Gamma = 275 \pm 35$  MeV, coupling to both  $^3S_1$  and  $^3D_1$ .

## 1 Introduction

The PS185 collaboration has made extensive measurements of  $\bar{p}p \rightarrow \bar{\Lambda}\Lambda$  at LEAR. Integrated cross sections have been measured at fine steps of momentum close to the  $\bar{\Lambda}\Lambda$  threshold [1-4]; Ref. [4] summarises results. Differential cross sections extend up to 1990 MeV/c. The decays of  $\Lambda$  and  $\bar{\Lambda}$  analyse their polarisation  $P_y = A_{00N0} = A_{000N}$  and measure spin correlations  $C_{NN}$ ,  $C_{SS}$ ,  $C_{LL}$  and  $C_{LS} = C_{SL}$  [5]. Data from a polarised target provide further measurements with target polarisation normal to the scattering plane [6].

An early partial wave analysis close to threshold was made by Tabakin et al. [7]. The objective here is to extend the partial wave analysis over the whole momentum range, including polarised target data.

There are six spin dependent amplitudes for  $\bar{p}p \rightarrow \bar{\Lambda}\Lambda$  [8], one more than for  $NN$  and  $\bar{N}N$  elastic scattering, where particles in initial and final states are identical. There are 6 further measurements from the polarised target. Firstly the asymmetry  $A_{0N00}$  from the polarised target is different to  $A_{00N0}$  because the nucleon and  $\Lambda$  are different particles. Secondly, there are rather precise measurements of spin transfer parameters  $D_{NN}$  and  $K_{NN}$ . Thirdly, the triple spin parameters  $C_{0NSS}$ ,  $C_{0NLS}$  and  $C_{0NSL}$  are independent measurements. Here, the first suffix refers to the  $\bar{p}$  beam, which is unpolarised, the second refers to the target proton, the third refers to the  $\bar{\Lambda}$  and the fourth refers to the  $\Lambda$ . Further measurements of  $C_{0NLL}$  and  $C_{0NNN}$  are redundant. Paschke and Quinn [9] show that  $C_{0NSS} = -C_{0NLL}$ , although

both sets of data can be included in the analysis, to improve statistics. Also  $A_{0NNN} = A_{0N00}$ ; the latter is much better determined than  $A_{0NNN}$ .

There is then a chance of determining the six amplitudes up to an overall unmeasurable phase. In principle eleven sets of data are sufficient providing they explore all amplitudes in an ideal way. In practice, it turns out that the determination is almost unique at 1637 MeV/c, the only momentum where polarised target data are available. There are some minor reservations concerning relative branchings to  ${}^3F_2$  and  ${}^3P_2$  and between  ${}^3D_1$  and  ${}^3S_1$ . It is necessary to apply a mild constraint to partial wave amplitudes for  ${}^3P_2 \rightarrow {}^3F_2$  and  ${}^3F_2 \rightarrow {}^3P_2$ , in order to prevent them drifting to large values. It is also necessary to make the simplifying assumption that, away from 1637 MeV/c,  ${}^3D_1 \rightarrow {}^3S_1$  and  ${}^3D_1 \rightarrow {}^3D_1$  amplitudes are related to  ${}^3S_1 \rightarrow {}^3S_1$  by simple centrifugal barrier factors. In the limited mass range over which data are available, these are mild assumptions, which have little effect on the determination of other partial waves.

The available mass range extends only 200 MeV above the  $\bar{\Lambda}\Lambda$  threshold. Resonances typically have widths of 250 MeV, so it is difficult to establish the presence of resonances from PS185 data alone. Nonetheless, results can be compared with analyses of Crystal Barrel and PS172 data having the same quantum numbers. In those data, a mass range of 500 MeV is available. For  $I = 0$ ,  $C = +1$ , there are seven sets of data from these two experiments for final states  $\pi^0\pi^0$ ,  $\eta\eta$ ,  $\eta\eta'$ ,  $\eta\pi^0\pi^0$ ,  $\eta'\pi^0\pi^0$ ,  $3\eta$  and  $\pi^-\pi^+$ ; in addition there is some information from the production process  $\bar{p}p \rightarrow (\eta\pi^0\pi^0)\eta$ . From those extensive data, many resonances are observed with securely determined parameters [10]. It is of interest to see if those resonances corresponds to structures observed in  $\bar{p}p \rightarrow \bar{\Lambda}\Lambda$ . That is quite likely, in the same way that  $J^P = 0^+$  resonances appear in both  $\pi\pi$  and  $K\bar{K}$  channels.

## 2 A cusp at the $\bar{\Lambda}\Lambda$ threshold

Fig. 1(a) shows integrated cross sections very close to threshold for  $\bar{p}p \rightarrow \bar{\Lambda}\Lambda$ . The curve shows the S-wave intensity deduced later from the partial wave analysis; the remaining intensity comes from P-waves in this mass range.

The cross section for the inverse process  $\bar{\Lambda}\Lambda \rightarrow \bar{p}p$  may be derived using detailed balance:

$$\sigma(\bar{\Lambda}\Lambda \rightarrow \bar{p}p) = (p/k)^2 \sigma(\bar{p}p \rightarrow \bar{\Lambda}\Lambda). \quad (1)$$

Here,  $p$  and  $k$  are momenta of  $p$  and  $\Lambda$  in the centre of mass frame. Fig. 1(b) shows the resulting cross sections for  $\bar{\Lambda}\Lambda \rightarrow \bar{p}p$ . There is a cusp at threshold, first reported in Ref. [11]. Cusps are in principle well known, but are not often seen, so this case is interesting.

The cusp is a feature of S-waves. The curve shows the fitted S-wave intensity; in this mass range, the difference from data is purely due to P-waves. These P-waves are surprisingly strong near threshold, but are very well determined from polarisations and forward-backward asymmetries in differential cross sections (Fig. 2 below). The PS185 collaboration makes the reasonable conjecture that the S-wave is strongly absorbed into other open channels, whereas in this mass range P-waves are highly peripheral and therefore suffer little attenuation from annihilation. Up to 6 MeV, P-waves have momenta  $k < 85$  MeV/c, and therefore a classical impact parameter  $> 2.3$  fm.

The curve follows the familiar  $1/v$  law of thermal neutron physics. The  $1/v$  dependence is verified in Fig. 1(c), where  $\sigma(\bar{\Lambda}\Lambda \rightarrow \bar{p}p) \times k$  is plotted after subtracting off the contributions from P-waves.

It will be useful to exhibit the origin of the cusp assuming there is an S-wave resonance, which will be fitted later to the data. The result is however quite general and is derived in the textbook of Landau and Lifshitz [12]. For an S-wave resonance, the partial wave amplitude is

$$f_s(\bar{p}p \rightarrow \bar{\Lambda}\Lambda) = \frac{1}{p} \frac{\sqrt{\Gamma_{\bar{p}p}(s)\Gamma_{\bar{\Lambda}\Lambda}(s)}}{D(s)}, \quad (2)$$

where  $D(s) = M^2 - s - m(s) - iM\Gamma_{tot}(s)$ ; the term  $m(s)$  in the denominator  $D(s)$  will be discussed below. Since  $\Gamma_{\bar{\Lambda}\Lambda} \propto k$  and  $\Gamma_{\bar{p}p} \propto p$  near threshold,

$$f_s(\bar{p}p \rightarrow \bar{\Lambda}\Lambda) \propto \frac{\sqrt{k/p}}{D(s)}. \quad (3)$$

The amplitude for  $\bar{\Lambda}\Lambda$  elastic scattering is

$$f_s(\bar{\Lambda}\Lambda \rightarrow \bar{\Lambda}\Lambda) = \frac{1}{k} \frac{\Gamma_{\bar{\Lambda}\Lambda}(s)}{D(s)}. \quad (4)$$

Apart from a slow energy dependence from  $D(s)$ , the amplitude goes to a constant at threshold, namely the scattering length  $a$ . The amplitude for

$\bar{\Lambda}\Lambda \rightarrow pp$  is

$$f_s(\bar{\Lambda}\Lambda \rightarrow \bar{p}p) = \frac{1}{k} \frac{\sqrt{\Gamma_{\bar{p}p}(s)\Gamma_{\bar{\Lambda}\Lambda}(s)}}{D(s)}, \quad (5)$$

and is proportional to  $(p/k)^{1/2}/D(s)$  at threshold. The intensity  $|f_s(\bar{\Lambda}\Lambda \rightarrow \bar{p}p)|^2 \propto 1/k$ , apart from the slowly varying factor  $p/|D(s)|^2$ . This is the origin of the  $1/v$  law.

At threshold there is a step in  $Im f_s(\bar{\Lambda}\Lambda \rightarrow \bar{\Lambda}\Lambda)$ . Associated with this step is a rapid variation of  $Re f_s(\bar{\Lambda}\Lambda \rightarrow \bar{\Lambda}\Lambda)$ , i.e. a dispersive effect. For a resonance,  $m(s)$  of eqn. (3) is given [13] by

$$m(s) = \frac{M^2 - s}{\pi} \int \frac{Im f_s(s') ds'}{(M^2 - s')(s' - s)}, \quad (6)$$

where a subtraction is made on resonance. This formula will be used in fitting an S-wave resonance to the data.

For higher partial waves, the centrifugal barrier makes cusp effects negligible.

### 3 Data and analysis procedures

Figs. 2–9 show the PS185 data, together with fits described here.

#### 3.1 Formulae for Observables and Partial wave amplitudes

Elchikh and Richard [8] show that six amplitudes are needed to describe  $\bar{p}p \rightarrow \bar{\Lambda}\Lambda$ . Formulae for observables are readily adapted from the well known expressions for  $NN$  elastic scattering [14]. They have also been written down by Paschke and Quinn [9]. However, one needs to be aware that Paschke and Quinn quantise along the same axes for initial and final states. Suppose the  $y$ -axis is taken normal to the scattering plane,  $z$  along the beam direction and  $x$  sideways in the plane of scattering. For spin transfer parameters, the expressions of Paschke and Quinn describe observables such as  $A_{0yxz}$ , with  $x$  and  $z$  in the *same* direction for initial and final states. The PS185 collaboration uses for the initial  $\bar{p}p$  state the same axes  $x, y, z$ . However, for the final state, they use axes  $x', y$  and  $z'$  with  $z'$  along the direction of

the final  $\bar{\Lambda}$ . It is necessary to allow for the rotation of spins through the scattering angle  $\theta$  between initial and final states. For triplet states, this involves a simple projection of spins as vectors from one set of axes to the other. For singlet states, the rotation of axes has no effect.

## 3.2 Parametrisation of Partial Wave Amplitudes

Partial wave amplitudes need to include three standard factors: (a) the  $1/p$  flux factor for the centre of mass momentum  $p$  in the  $\bar{p}p$  channel, (b) the relativistic phase space factor  $\sqrt{\rho_1} = (2p/\sqrt{s})^{1/2}$  for the  $\bar{p}p$  channel and the factor  $(2k/\sqrt{s})^{1/2}$  for  $\bar{\Lambda}\Lambda$ , (c) Blatt-Weiskopf centrifugal barrier factors for both  $\bar{p}p$  and  $\bar{\Lambda}\Lambda$  channels [15]; they give the required  $k^L$  dependence near threshold on angular momentum  $L$  and momentum  $k$  is the  $\bar{\Lambda}\Lambda$  channel. The product of these three factors will be written as  $G(s)$ . Then partial wave amplitudes for spin  $J$ , angular momenta  $\ell$  and  $L$  in initial and final states  $F_{J,\ell,L}(s)$  are written:

$$F_{J,\ell,L}(s) = G_{J,\ell,L}(s)f_{J,\ell,L}(s), \quad (7)$$

where  $f(s)$  are analytic functions. Note that the factor  $G(s)$  must be factored out in order to avoid branch cuts below threshold.

Data at 1637 MeV/c are adequate to give a unique set of partial waves. At other momenta, the analysis reveals quickly that the transition amplitude  ${}^3S_1 \rightarrow {}^3D_1$  is well determined by the polarisations of  $\Lambda$  and  $\bar{\Lambda}$ . The data are consistent with the same  $s$ -dependence for this amplitude as for  ${}^3S_1 \rightarrow {}^3S_1$ , except for the centrifugal barrier factor for the D-wave. The radius of the centrifugal barrier optimises at  $R = 1.1$  fm. To simplify the analysis, the  ${}^3S_1 \rightarrow {}^3S_1$  amplitude is parametrised with coupling constant  $g_1$  and the  ${}^3S_1 \rightarrow {}^3D_1$  transition amplitude is parametrised with coupling constant  $g_1 h_1$ , where  $h_1$  is a complex constant.

The separation between  ${}^3D_1$  and  ${}^3S_1$  initial states is sensitive only to polarised target data. Therefore, the  ${}^3D_1 \rightarrow {}^3S_1$  amplitude is parametrised with coupling constant  $g_1 h'_1$ , and it is necessary to assume that  $h'_1$  does not vary with  $s$ . The same is true for the  ${}^3D_1 \rightarrow {}^3D_1$  amplitude which is fitted with coupling constant  $g_1 h''_1$  with  $h''_1$  constant. Physically, the implication is that the branching ratio of  $\bar{\Lambda}\Lambda$  does not change with mass. These assumption are of little consequence at low momenta because the  $L = 2$  centrifugal barrier suppresses the amplitude near threshold for initial D-states.

Partial waves for  $2^+$ ,  $3^-$  and  $4^+$  are treated in the same way. Care is needed even at 1637 MeV/c in handling the amplitude for  ${}^3F_2 \rightarrow {}^3P_2$ . With present data, the separation of the four  $2^+$  amplitudes, abbreviated as  $f_{PP}$ ,  $f_{PF}$ ,  $f_{FP}$  and  $f_{FF}$ , is the weakest link in the entire analysis. The  $f_{FF}$  amplitude is small and not a matter for concern. The  $f_{PF}$  amplitude is well determined by polarisations of  $\Lambda$  and  $\bar{\Lambda}$  and differential cross sections. However, the  $f_{FP}$  amplitude shows some tendency to drift upwards in magnitude with only a small change in  $\chi^2$ . The problem is cured by including into  $\chi^2$  a weak penalty function which limits its magnitude. The penalty function adds to  $\chi^2$  a term

$$\Delta\chi^2 = \frac{|f_{FP}|^2}{\Delta_{FP}^2},$$

and the denominator  $\Delta_{FP}^2$  is adjusted so that this term contributes 9 to  $\chi^2$ . This technique allows  $F_{FP}$  to grow if the data really demands it, but constrains it from running away with little change in  $\chi^2$ . Below 1637 MeV/c, the fit is insensitive to this restriction, but above 1637 MeV/c, there may be some sensitivity. Further data from a polarised target at high momentum would solve this possible problem.

For  $J^P = 3^-$  and  $4^+$ , contributions from  ${}^3G_3 \rightarrow {}^3G_3$ ,  ${}^3D_3 \rightarrow {}^3G_3$  and  ${}^3F_4 \rightarrow {}^3H_4$  are negligible because of centrifugal barriers in  $\bar{\Lambda}\Lambda$ . Both the inverse amplitudes  ${}^3G_3(\bar{p}p) \rightarrow {}^3D_3(\bar{\Lambda}\Lambda)$  and  ${}^3H_4 \rightarrow {}^3F_4$  are definitely required. Surprisingly, the  ${}^3G_4 \rightarrow {}^3G_4$  is also definitely required;  $5^-$  amplitudes are negligible.

Table 1 shows changes in  $\chi^2$  when partial waves are removed from the final fit one by one and remaining amplitudes are re-optimised. The singlet partial waves  ${}^1S_0$  and  ${}^1P_1$  are very small, as the PS185 collaboration found earlier. Any partial waves affecting  $\chi^2$  by  $< 10$  are eliminated.

The initial fits take  $f_J(s)$  to be constants (where possible) or linear with  $s$ , except for the threshold cusp. In no case does the phase decrease with  $s$ . In several partial waves, large linear terms were required, producing phase variations of order  $90^\circ$ . An empirical linear fit to the phase begs the question where the phase originates. It rapidly became apparent that better fits could be obtained by allowing a resonant phase variation in some partial waves.

A resonance with a large width gives an essentially linear phase variation. Therefore the final analysis uses constant amplitudes plus a resonant form for

Amplitude	Change in $\chi^2$
${}^3S_1 \rightarrow {}^3S_1$	1894
${}^3S_1 \rightarrow {}^3D_1$	271
${}^3D_1 \rightarrow {}^3S_1$	56
${}^3D_1 \rightarrow {}^3D_1$	50
${}^3P_0$	98
${}^3P_1$	248
${}^3P_2 \rightarrow {}^3P_2$	1337
${}^3P_2 \rightarrow {}^3F_2$	69
${}^3F_2 \rightarrow {}^3P_2$	749
${}^3F_2 \rightarrow {}^3F_2$	34
${}^3D_2$	51
${}^3D_3 \rightarrow {}^3D_3$	681
${}^3G_3 \rightarrow {}^3D_3$	177
${}^3F_3$	242
${}^3F_4 \rightarrow {}^3F_4$	684
${}^3H_4 \rightarrow {}^3F_4$	111
${}^3G_4$	108
${}^1S_0$	15
${}^1P_1$	25

Table 1: Changes in  $\chi^2$  when individual partial waves are dropped from the fit and other amplitudes are re-optimised.

all partial waves, though allowing the resonance width to go to a large value if the data prefer the linear phase variation. This allows a rather flexible parametrisation of the  $s$ -dependence.

In the final fit, the cusp in the  ${}^3S_1$  amplitude is fitted by taking the amplitude

$$f = \frac{1}{M^2 - s - m(s) - iM[\Gamma_0 + \Gamma_{\bar{\Lambda}\Lambda}(s)]}, \quad (8)$$

$$\Gamma_{\bar{\Lambda}\Lambda} = C\sqrt{1 - 4M_\Lambda^2/s}, \quad (9)$$

and taking  $m(s)$  from eqn. (6). The magnitude of the constant  $C$  in the  $\Lambda\Lambda$

width is adjusted so as to reproduce the observed total intensity of the  $^3S_1$  and  $^3D_1$  partial waves, and using the same  $C$  for coupling to  $\bar{p}p$  and  $\bar{\Lambda}\Lambda$ .

## 4 Results

The  $\chi^2$  of the fit is 1377 for 1201 data points and 61 fitted parameters. This is a similar quality of fit to partial wave analyses of  $NN$  elastic scattering data.

A technical detail is that normalisations of each set of differential cross sections and integrated cross sections are varied in accordance with their published normalisations. This smooths out some scatter amongst the points, but has negligible effect on fitted amplitudes. It turns out to be unnecessary to allow normalisations of polarisation data to adjust in this way.

Fig. 10 shows the intensities of each partial wave in the integrated cross section. They are plotted against the mass above the  $\bar{\Lambda}\Lambda$  threshold:  $\Delta M = M - 2M_\Lambda$ . These intensities contain  $G^2(s)$ , i.e. the flux and phase space factors and centrifugal barriers.

It is more instructive to view  $|f_J(s)|^2$ , where the kinematic factor  $G^2$  is omitted. These are shown in Fig. 11. One further factor is also removed. Each amplitude has Clebsch-Gordan coefficients which affect the contributions to integrated cross sections. These factors are listed in Table 2 and are also factored out in drawing Fig. 11. The results shows matrix elements squared, unencumbered by kinematic factors or spin-coupling factors.

A question is how reliable these intensities are. A general conclusion is that the final angular momentum state is well determined by polarisations in the final state. Hence  $^3S_1 \rightarrow ^3D_1$  and  $^3P_2 \rightarrow ^3F_2$  intensities are well determined. In a variety of fits with different combinations of amplitudes and different assumptions for the fitting functions  $f_J(s)$  and centrifugal barriers, fluctuations  $< 10\%$  are observed. However, identification of the initial state depends on polarised target data. Hence the intensities of  $^3F_2 \rightarrow ^3P_2$  and  $^3D_1 \rightarrow ^3S_1$  partial waves are well determined ( $\pm 7\%$ ) at 1637 MeV/c, but their  $s$ -dependence away from this mass is uncertain. Some limitations arise from accurate measurements of differential cross sections and polarisations, but one should not draw conclusions from the  $s$ -dependence of intensities for  $^3F_2 \rightarrow ^3P_2$  or  $^3D_1 \rightarrow ^3S_1$ . On Figs. 10 and 11, this  $s$ -dependence is dictated by the centrifugal barriers.



Amplitudes	spin factors
${}^3S_1, {}^3S_1 \rightarrow {}^3D_1$	3
${}^3D_1, {}^3D_1 \rightarrow {}^3S_1$	3/5
${}^3P_0$	1/3
${}^3P_1, {}^3D_2, {}^3F_3, {}^3G_4$	1
${}^3P_2, {}^3P_2 \rightarrow {}^3F_2$	5/3
${}^3F_2, {}^3F_2 \rightarrow {}^3P_2$	5/7
${}^3D_3$	7/5
${}^3F_4$	9/7
${}^3G_3 \rightarrow {}^3D_3$	7/9

Table 2: Spin weighting of amplitudes in integrated cross sections.

The top row of Fig. 11 shows  $1^{--}$  intensities. There is a distinct maximum  $\sim 60$  MeV above threshold, i.e. at a mass of 2290 MeV. It is stronger in  ${}^3D_1 \rightarrow {}^3D_1$  than in  ${}^3S_1 \rightarrow {}^3S_1$ . This peak eventually requires interpretation as a resonance.

The second row of Fig. 11 shows  $2^{+}$  intensities. The  ${}^3P_2 \rightarrow {}^3P_2$  and  ${}^3F_2 \rightarrow {}^3F_2$  results are featureless, and the latter is quite small. However, the  ${}^3P_2 \rightarrow {}^3F_2$  amplitude grows quite strongly with mass. It is well determined by polarisations in the  $\bar{\Lambda}\Lambda$  final state.

The  ${}^3P_0$  and  ${}^3F_3$  intensities show distinct peaks which will later be associated with known resonances in Crystal Barrel  $I = 0$ ,  $C = +1$  amplitude analyses. The  ${}^3D_3 \rightarrow {}^3D_3$  and  ${}^3G_3 \rightarrow {}^3D_3$  intensities likewise show peaks which may be associated with a known resonance. The  ${}^3G_3 \rightarrow {}^3D_3$  amplitude is well determined only by polarised target data, so the peak in its intensity follows from the assumption that it scales from the  ${}^3D_3 \rightarrow {}^3D_3$  amplitude. The shift between the peaks arises from a mild sensitivity to differential cross sections at high mass, and may not be reliable.

The  ${}^3P_1$  and  ${}^3D_2$  amplitudes of Fig. 11 drop from threshold and cannot be associated with resonant structure. However, the  ${}^3D_2$  amplitude is small, and it will fit with very little change in  $\chi^2$  to the known  ${}^3D_2$  resonance  $\rho_2(2195)$  [16]. The  ${}^3F_4$  intensity rises steadily with mass and shows no indication of the known  $f_4(2300)$  resonance [17].

The peaks in  ${}^3P_0$ ,  ${}^3D_3$  and  ${}^3F_3$  fit naturally as resonances. Fig. 12 shows

Argand diagrams. There are clear loops for these partial waves. Table 3 shows fitted masses and widths in columns 2 and 3. Errors cover both statistical variations and systematic variations over a variety of fits with different assumptions (e.g. concerning centrifugal barriers and small amplitudes). In all cases, statistical errors are roughly 35–50% of systematic errors. Around the optimum, both mass and width show well defined parabolic minima in  $\chi^2$ . For the  $1^{--}$  resonance in Table 3,  $\Gamma_0$  of eqn. (8) is 260 MeV and  $\Gamma_{\bar{\Lambda}\Lambda} = 15$  MeV on resonance, leading to a tabulated width of 275 MeV.

The next two columns compare with known resonances observed in Crystal Barrel data [10,16]. Parameters are remarkably close. If the masses and widths of columns 4 and 5 are used in the fit, the change in  $\chi^2$  is only 12, and 6 parameters become fixed. It therefore looks very likely that the same resonances appear in PS185 data.

$J^{PC}$	$M(\text{MeV})$	$\Gamma(\text{MeV})$	$M(\text{MeV})$	$\Gamma(\text{MeV})$
$0^{++}$	$2314 \pm 25$	$144 \pm 20$	$2337 \pm 14$	$217 \pm 33$
$2^{++}$	$2387 \pm 35$	$33 \pm 100$	-	-
$3^{++}$	$2334 \pm 25$	$200 \pm 20$	$2303 \pm 15$	$214 \pm 29$
$3^{--}$	$2278 \pm 28$	$224 \pm 50$	$2255 \pm 15$	$175 \pm 30$
$1^{--}$	$2290 \pm 20$	$275 \pm 30$	-	-

Table 3: Columns 2 and 3 show resonance parameters from PS185 data; columns 4 and 5 show comparisons with Crystal Barrel results [10,16].

There is a further feature which agrees with earlier observation of the  $3^-$  resonance. In Fig. 11, there is a highly significant  $^3G_3 \rightarrow ^3D_3$  intensity. The requirement for this amplitude arises from  $D_{NN}$  and  $K_{NN}$  data: dashed curves on Fig. 8 show the worse fit without this amplitude. In Ref. [16], a strong  $^3G_3$  resonance was likewise observed at 2255 MeV. In this mass range, both a  $^3D_3$  and a  $^3G_3$  resonance are expected in conventional quark models. So it is quite likely that two unresolved  $^3D_3$  and  $^3G_3$  resonance appear in both PS185 and Crystal Barrel data. In the Crystal Barrel analysis, a second state coupling mostly to  $^3D_3$  was reported at  $2285 \pm 60$  MeV with  $\Gamma = 230 \pm 40$  MeV.

There is also a possible identification of the  $2^+$  structure. There is a known  $f_2(1950)$  [17] with a large width of 500 MeV. If it is substituted into

the fit, there is almost no change in  $\chi^2$  and a small movement downwards of the  $2^+$  resonance of Table 3 to 2362 MeV. It is possible that this resonance is to be identified with the  $f_2(2339)$  of Etkin et al. in  $\pi\pi \rightarrow \phi\phi$  [18]; its appearance in the  $\bar{\Lambda}\Lambda$  channel would not be surprising. If the  $f_2(2339)$  is substituted into the fit with the width reported by Etkin et al,  $\chi^2$  changes by  $< 5$ .

The peak in  $^3S_1$  and  $^3D_1$  at 2290 MeV requires a strong phase variation. If the other peaks described above are identified with known resonances in Crystal Barrel data, it is inescapable that the  $1^{--}$  peak is resonant. It would be a new resonance. In the Crystal Barrel analysis of  $\omega\eta$ ,  $\omega\pi^0\pi^0$  and  $\pi^-\pi^+$  channels, the  $1^{--}$  amplitude was not well defined in this mass range. A resonance at this mass is a natural radial excitation of  $\omega_3(1670)$  [17] and  $\omega_3(1945)$  [16].

## 5 Some general remarks

In earlier work, attempts have been made to fit these and  $\bar{p}p$  elastic scattering data in terms of meson exchanges. There is no conflict between this approach and the appearance of resonances. Meson exchanges can act as part of the driving forces which generate resonances. When a resonance appears, the projection of the meson exchange into an individual partial wave acquires the resonance phase through re-scattering effects. A well known example of this is the nucleon exchange term which partially drives the formation of the  $\Delta(1232)$ . Chew and Low showed in 1956 how to include the nucleon exchange term in an effective range formula which includes the resonance [19].

A little information can be added concerning  $\bar{p}p \rightarrow \bar{\Lambda}\Sigma^0$ . Data for the integrated cross section for this process were reported in Ref. [4] close to threshold. It is of interest to use detailed balance as in Section 2 to derive the cross section for the inverse process  $\bar{\Lambda}\Sigma^0 \rightarrow \bar{p}p$ . Does a cusp appear at threshold? Results are displayed in Fig. 13.

Errors are sizable, but there is no clear evidence for a cusp. The PS185 publication remarks that there is evidence for strong P-waves very close to threshold. They are reported to be even stronger than those in  $\bar{p}p \rightarrow \bar{\Lambda}\Lambda$ . It seems likely that they obscure the presence of a cusp. A fit is shown using a sum of S and P waves, but there is considerably flexibility in their relative contributions.

Further progress depends on more data. It would be valuable to have polarised target data at other momenta, particularly towards the top of the mass range, e.g. at 1990 MeV/c. In principle, such a measurement is feasible at the new  $\bar{p}p$  ring planned at GSI. With a frozen spin target, such a measurement is technically straightforward. Using a detector such as Crystal Barrel, it would also be possible to make valuable polarisation measurements for channels such as  $\omega\pi$ ,  $\omega\eta$  and  $3\pi^0$ , allowing a definitive conclusion to the analysis of Crystal Barrel data. If a trigger could be included on  $K_S^0$  decays and/or  $K_L^0$  interactions in the detector, it would open up the possibility of studying final states such as  $K\bar{K}$ ,  $K\bar{K}\pi$  and  $K\bar{K}\pi\pi$  over a wide mass range, and hence extending the important LASS data, which run out around 2100 MeV.

## 6 Summary

A partial wave analysis has been presented of all published PS185 data. At 1637 MeV/c, the solution is unique, although care is needed to restrict the amplitude for  ${}^3F_2 \rightarrow {}^3P_2$  so that it does not drift away to a large value. The analysis may be extended to cover all other momenta by making the assumption that the  ${}^3D_1 \rightarrow {}^3S_1$  and  ${}^3D_1 \rightarrow {}^3D_1$  amplitudes are related to  ${}^3S_1 \rightarrow {}^3S_1$  simply by the centrifugal barrier for the initial state. The same assumption is employed for initial  $\bar{p}p$  states  ${}^3F_2$  and  ${}^3G_3$ . Below 1637 MeV/c, this assumption is not serious, since the centrifugal barriers for the initial state suppress these amplitudes strongly.

There is direct evidence for a cusp at threshold in  $\bar{\Lambda}\Lambda \rightarrow \bar{p}p$ . This cusp needs to be included into the treatment of the  ${}^3S_1$  partial waves.

There is evidence for large phase variations in several partial waves in Fig. 12. If resonances are fitted to  $0^{++}$ ,  $3^{++}$  and  $3^{--}$  partial waves, observed resonance parameters are remarkably close to resonances reported earlier in Crystal Barrel data. With that identification, a new  $1^{--}$  resonance is required at 2290 MeV. Also in  ${}^3P_2 \rightarrow {}^3F_2$ , there is evidence for a resonance around 2360 MeV which fits well as the  $f_2(2339)$  reported by Etkin et al.

## 7 Acknowledgments

I am grateful to Prof. T. Johansson for providing tables of final data. Also to Dr. K. Paschke and Dr. B. Quinn for extensive discussions on formulae for observables.

## References

- [1] P.D. Barnes et al., Phys. Lett. B189 (1987) 249.
- [2] P.D. Barnes et al., Phys. Lett. B229 (1989) 432.
- [3] P.D. Barnes et al., Phys. Lett. B331 (1994) 203.
- [4] P.D. Barnes et al., Phys. Rev. C62 (2000) 055203.
- [5] P.D. Barnes et al., Nucl. Phys. A526 (1991) 575.
- [6] B. Bassalleck et al., Phys. Rev. Lett. 89 (2002) 212302.
- [7] F. Tabakin, R.A. Eisenstein and Y. Lu, Phys. Rev. C44 (1991) 1749.
- [8] M. Elchikh and J.-M. Richard, Phys. Rev. C61 (2000) 035205.
- [9] K.D. Paschke and B. Quinn, Phys. Lett. B495 (2000) 49.
- [10] A.V. Anisovich et al., Phys. Lett. B491 (2000) 47.
- [11] D.V. Bugg, *Reinterpreting several narrow 'resonances' at threshold cusps*, submitted to Phys. Lett. B.
- [12] L.D. Landau and E.M. Lifshitz, *Quantum Mechanics*, Pergamon Press, London, 1959, pp 438-440.
- [13] N.A. Törnqvist, Z. Phys. C 68 (1995) 647.
- [14] N. Hoshizaki, Suppl. Progr. Theor. Phys. 42 (1968) 107.
- [15] D.V. Bugg, A.V. Sarantsev and B.S. Zou, Nucl. Phys. B471 (1996) 59.
- [16] A.V. Anisovich et al., Phys. Lett. B542 (2002) 19.

- [17] Particle Data Group, Phys. Rev. D66 (2002) 1.
- [18] A. Etkin et al., Phys. Lett. B201 (1988) 568.
- [19] G.F. Chew and F.E. Low, Phys. Rev. 101 (1956) 1570.

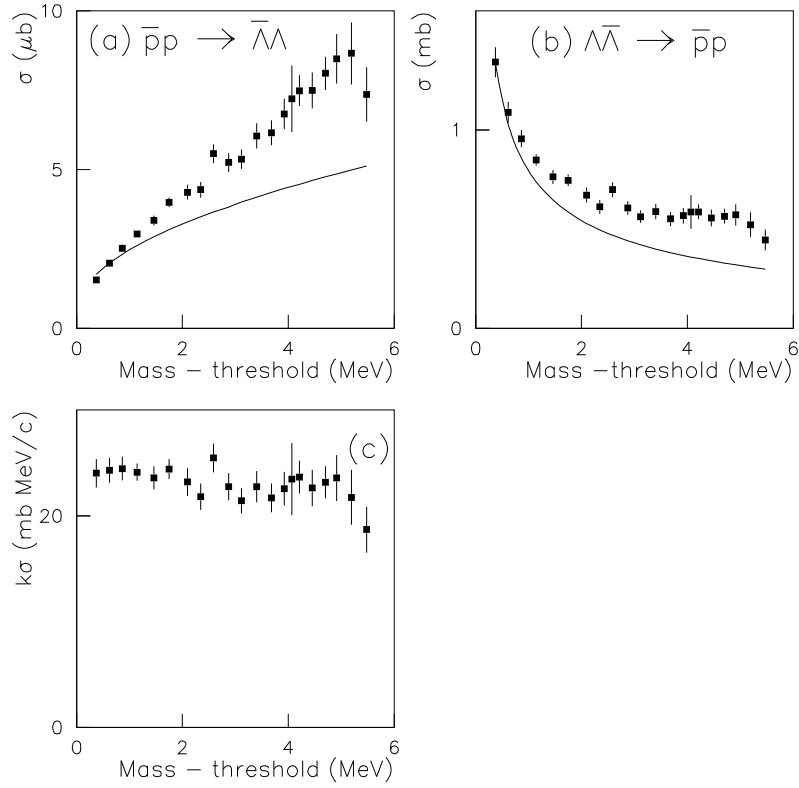


Figure 1: (a) Integrated cross sections for  $\bar{p}p \rightarrow \bar{\Lambda}\Lambda$ ; the curve shows the S-wave cross section from the amplitude analysis; (b) the corresponding cross section for  $\bar{\Lambda}\Lambda \rightarrow \bar{p}p$ ; the curve is the fitted S-wave intensity; (c)  $\sigma(\bar{\Lambda}\Lambda \rightarrow \bar{p}p) \times k$  v. excitation energy, after subtracting the P-wave intensity .

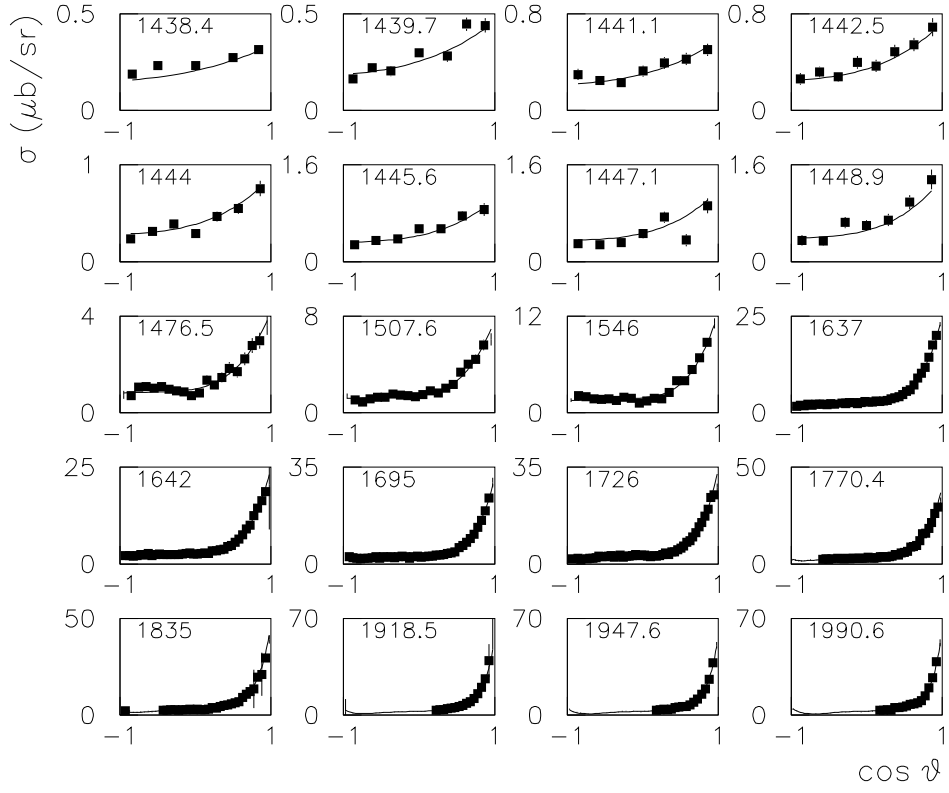


Figure 2: Fit to differential cross sections for  $\bar{p}p \rightarrow \bar{\Lambda}\Lambda$ ; lab momenta are indicated in each panel in MeV/c.



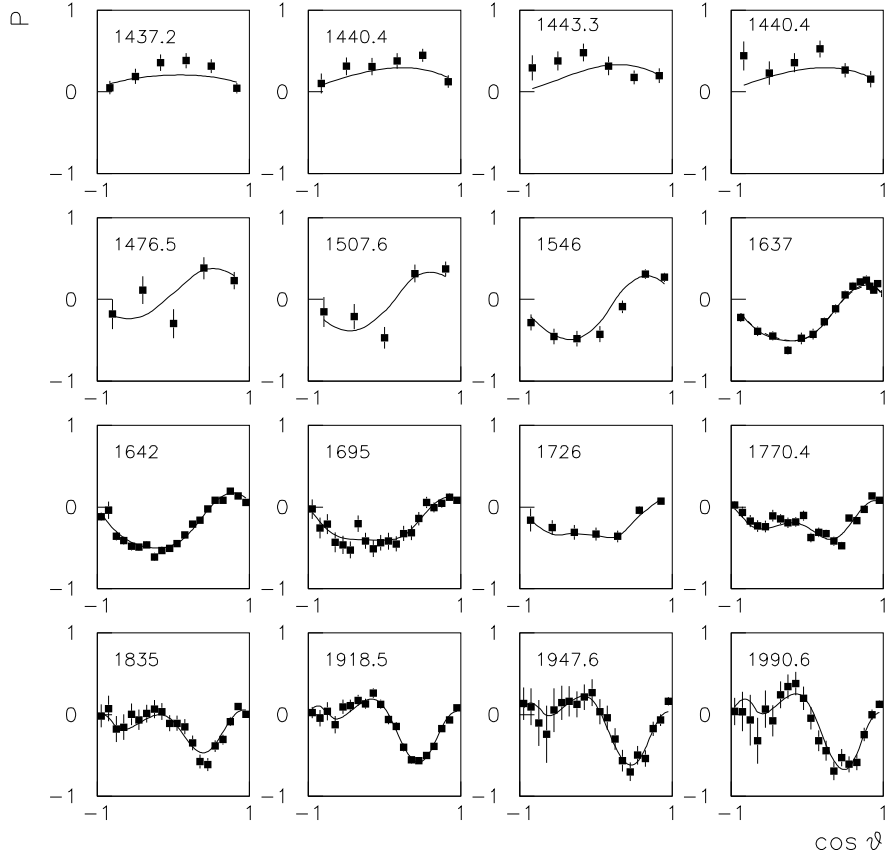


Figure 3: Fit to hyperon polarisations  $P_y$  for  $\bar{p}p \rightarrow \bar{\Lambda}\Lambda$ .

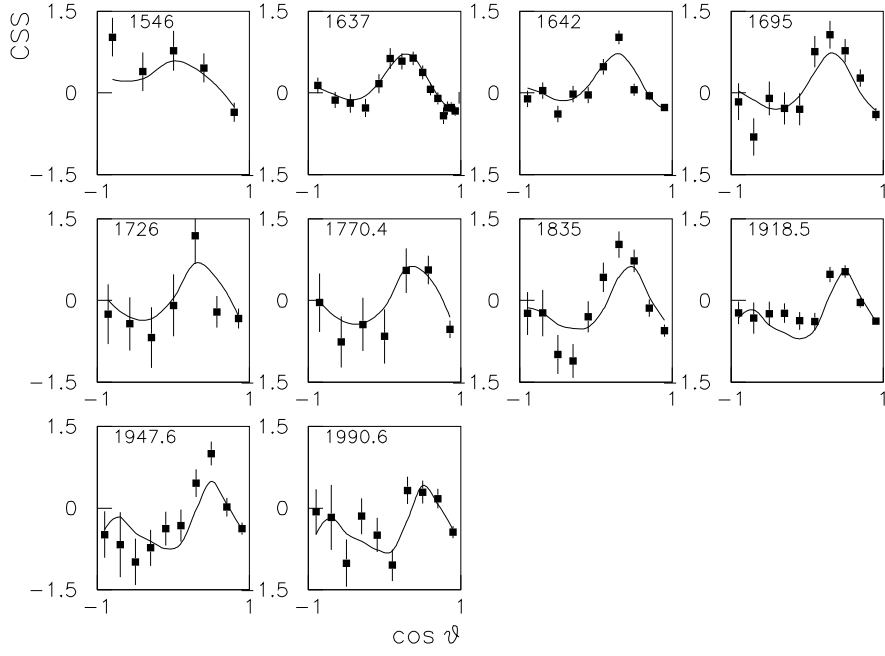


Figure 4: Fit to the spin correlation parameter  $C_{SS}$  for  $\bar{p}p \rightarrow \bar{\Lambda}\Lambda$ ;  $S$  is the component of spin transverse to the beam and in the plane of scattering.

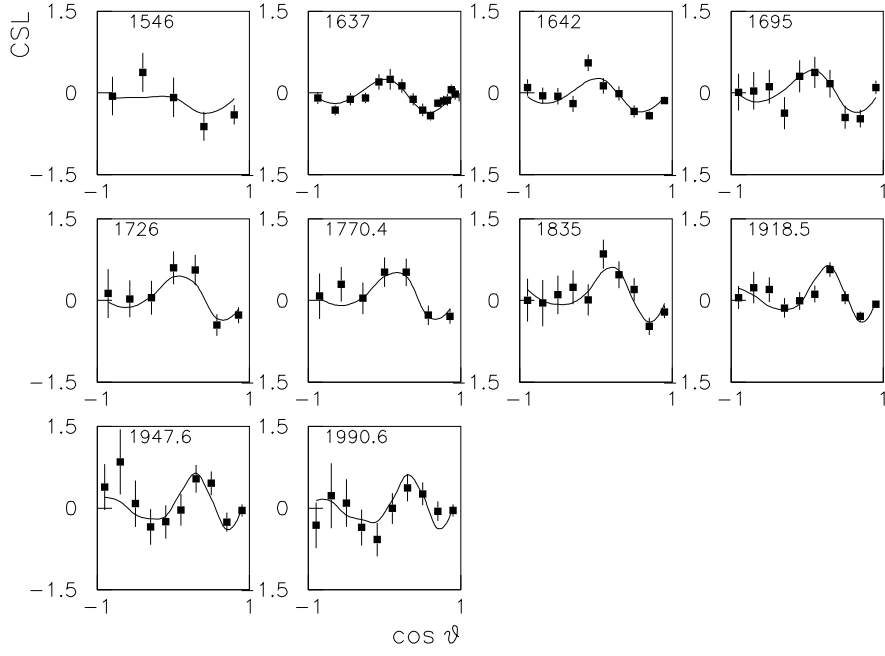


Figure 5: Fit to the spin correlation parameter  $C_{SL}$  for  $\bar{p}p \rightarrow \bar{\Lambda}\Lambda$ ;  $S$  is as in Fig. 4 and  $L$  is the longitudinal component of spin.

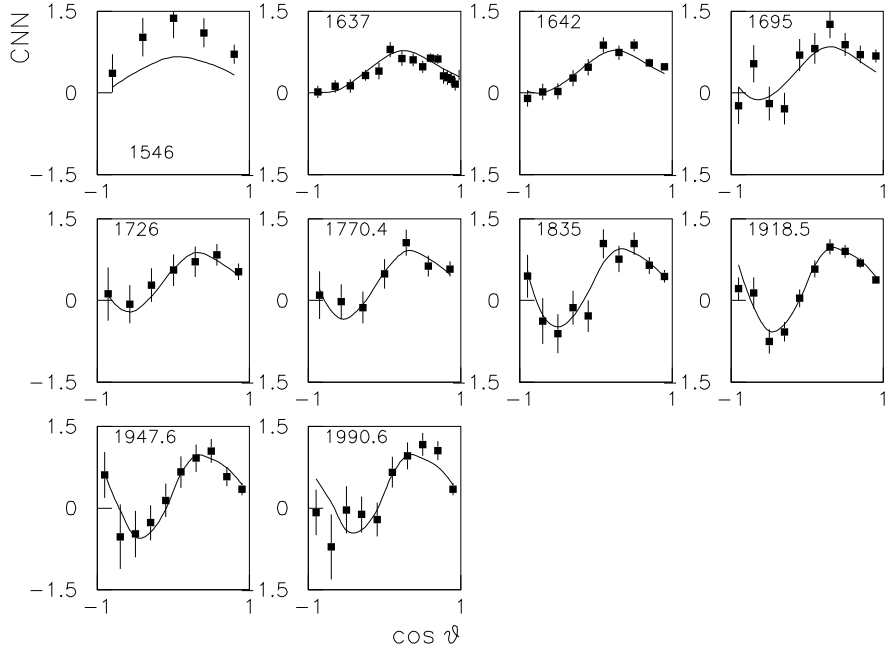


Figure 6: Fit to spin correlation parameter  $C_{NN}$  for  $\bar{p}p \rightarrow \bar{\Lambda}\Lambda$ ;  $N$  is the component of spin normal to the scattering plane.

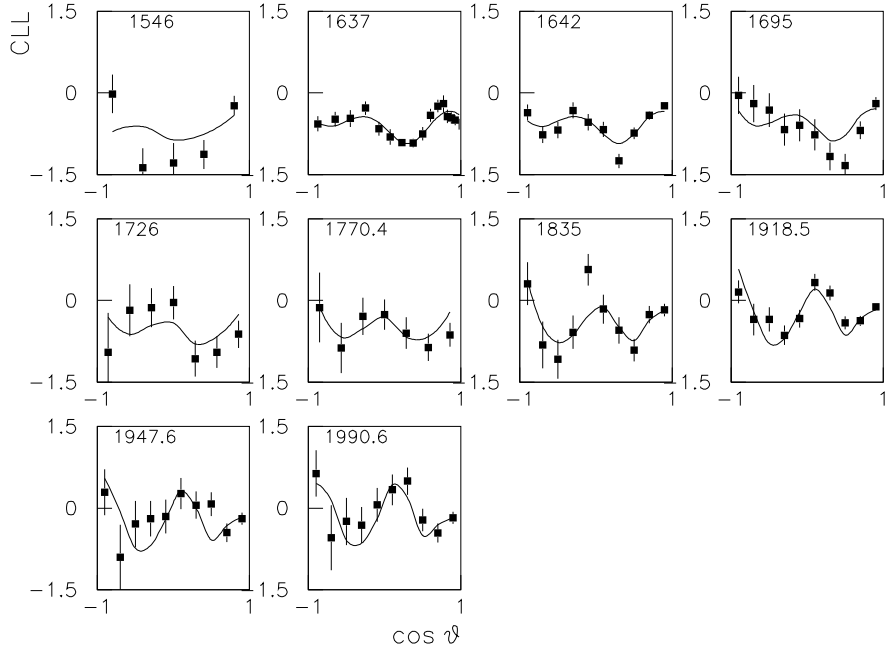


Figure 7: Fit to spin correlation parameters  $C_{LL}$  for  $\bar{p}p \rightarrow \bar{\Lambda}\Lambda$ ;  $L$  is the longitudinal component of spin.

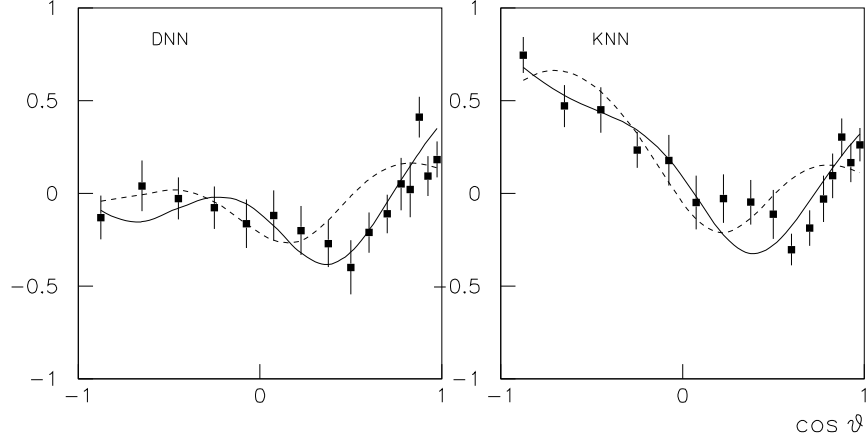


Figure 8: Fit to spin transfer parameters for  $\bar{p}p \rightarrow \bar{\Lambda}\Lambda$ ;  $D$  refers to spin transfer from proton to  $\Lambda$  and  $K$  to spin transfer from proton to  $\bar{\Lambda}$ ; the dashed curve shows the fit omitting the  $^3G_3 \rightarrow ^3D_3$  amplitude; data are at a beam momentum of 1637 MeV/c.

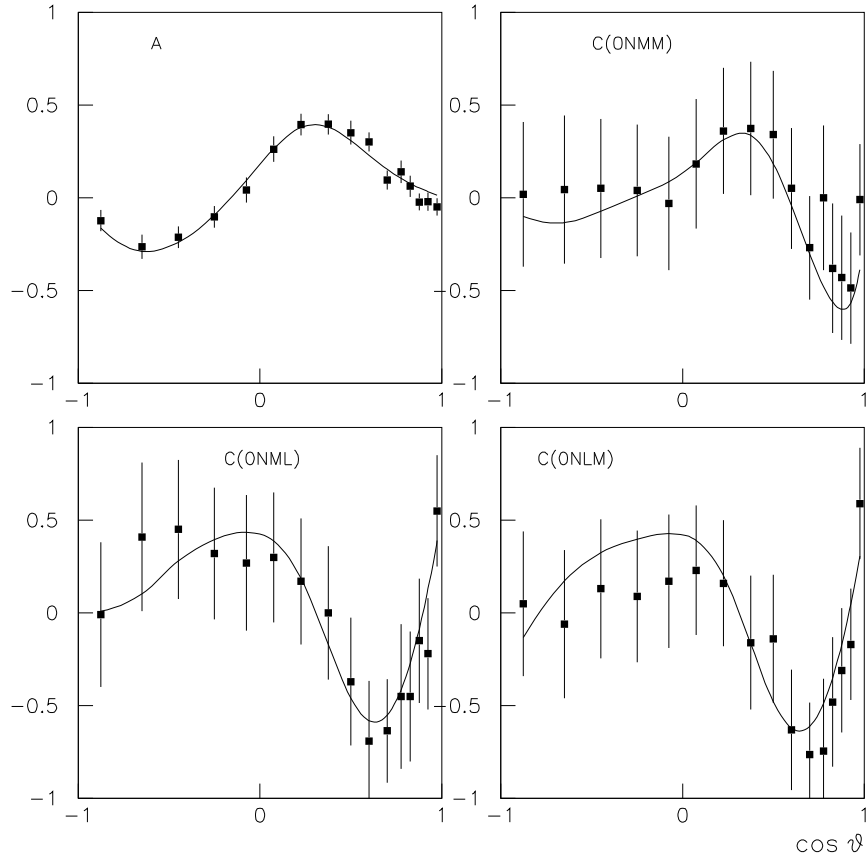


Figure 9: Fit to the asymmetry  $A$  from the polarised target for  $\bar{p}p \rightarrow \bar{\Lambda}\Lambda$  and to triple spin parameters. Data are at a beam momentum of 1637 MeV/c.

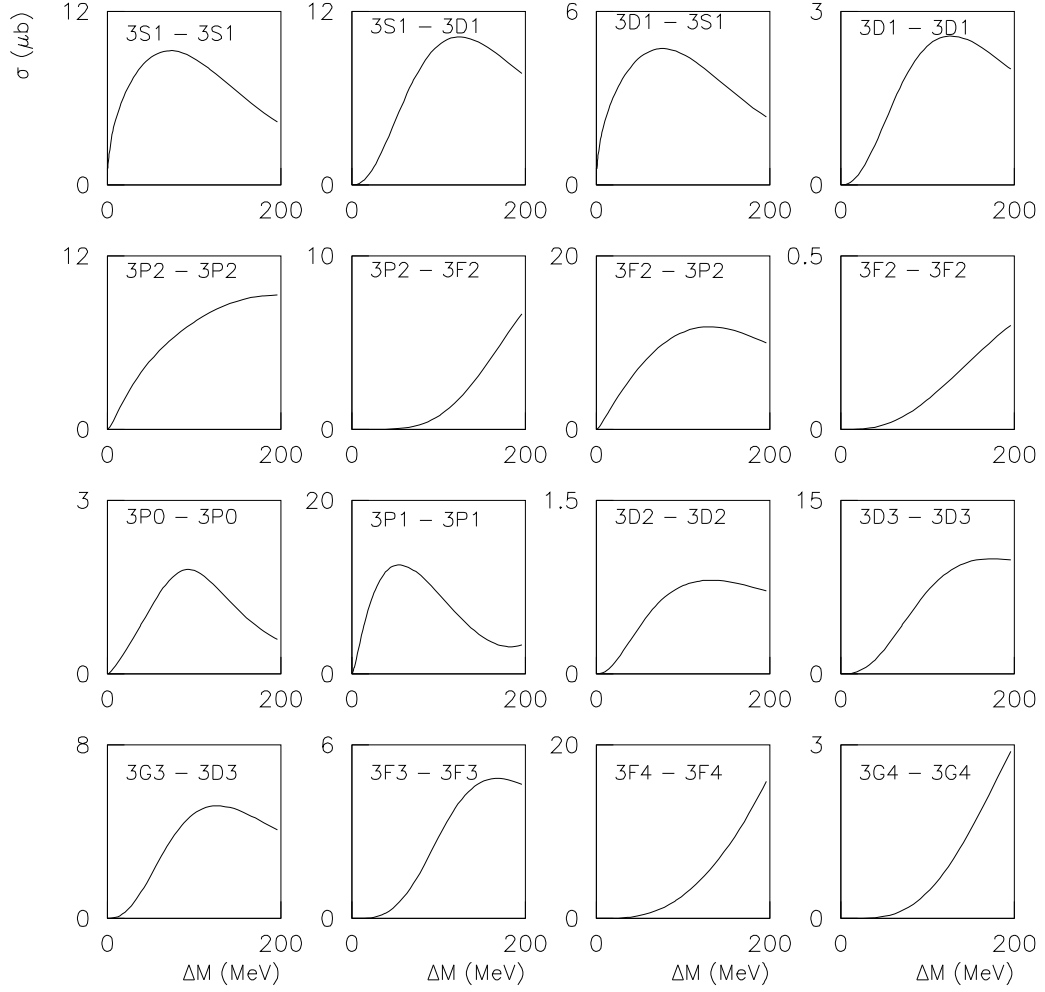


Figure 10: Contributions of partial wave amplitudes to the integrated cross section; a beam momentum of 1637 MeV/c corresponds to  $\Delta M = 71$  MeV,  $M = 2302.5$  MeV.



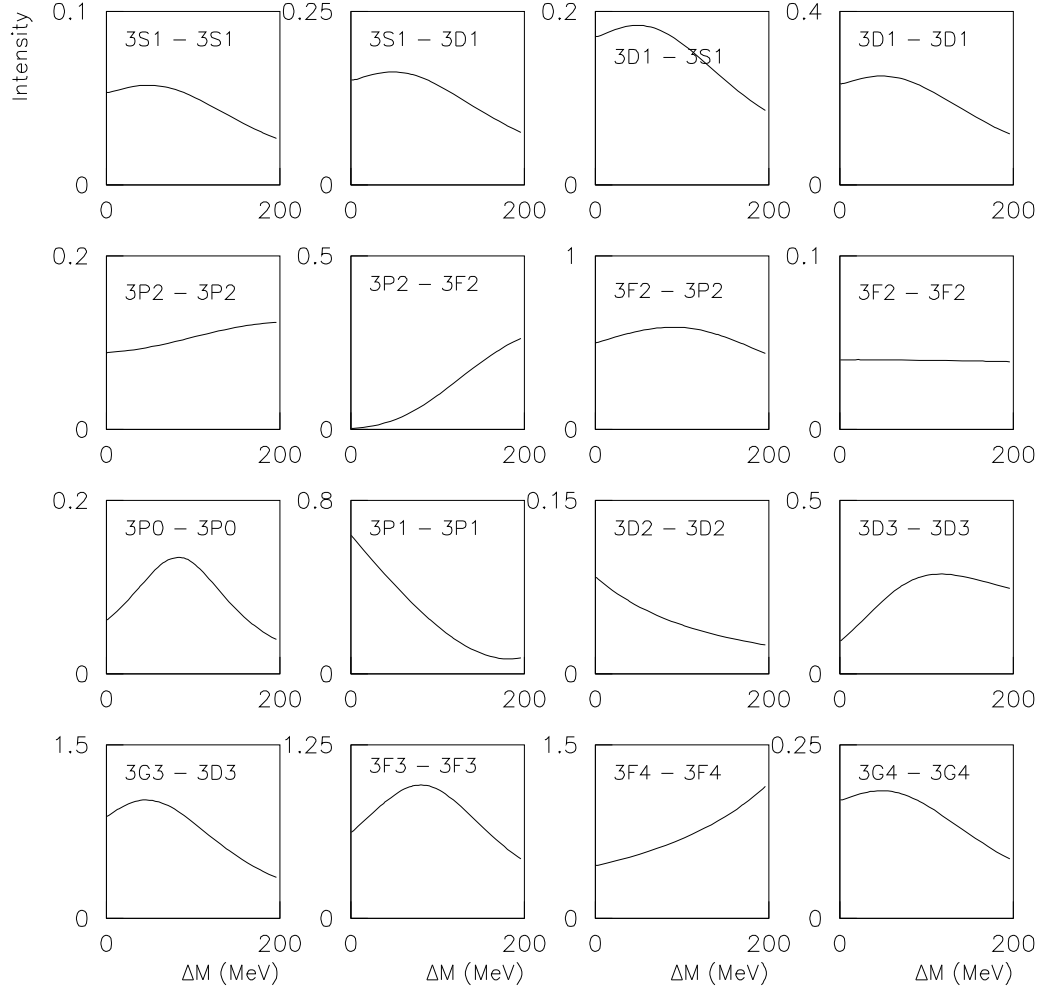


Figure 11: Magnitudes of  $|f_J(s)|^2$ , i.e. with the kinematic factor  $G^2(s)$  removed; a beam momentum of 1637 MeV/c corresponds to  $\Delta M = 71$  MeV,  $M = 2302.5$  MeV.

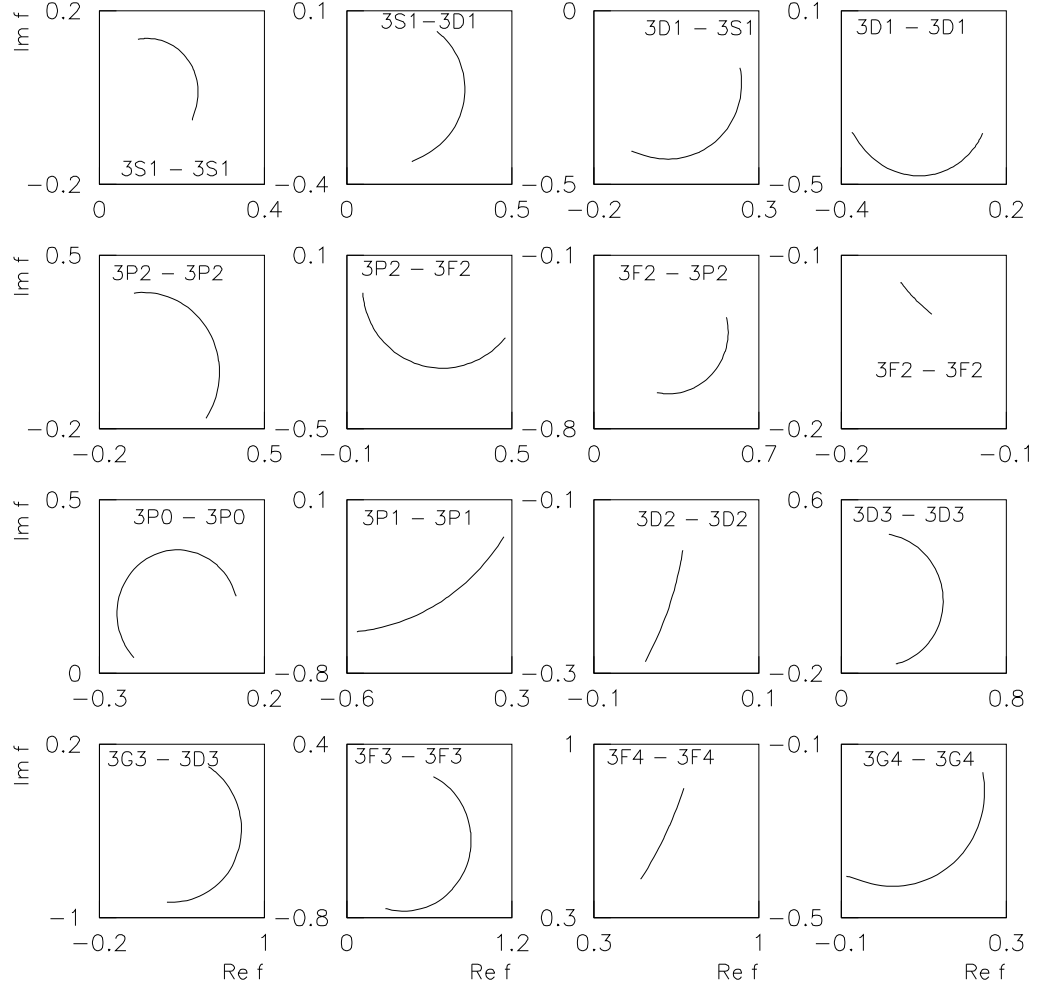


Figure 12: Argand diagrams for  $f_J(s)$ , i.e. after factoring out the kinematic factor  $G(s)$ .

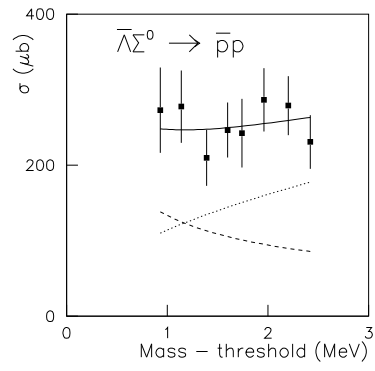


Figure 13: Integrated cross sections for  $\bar{\Lambda}\Sigma^0 \rightarrow \bar{p}p$  deduced from data of Ref. [4]; the full curve shows a fit to S and P waves, which are shown individually by the dotted (S) and dashed (P) curves.